remote sensing

MDPI

Article

An Improved RFI Mitigation Approach for SAR Based on Low-Rank Sparse Decomposition: From the Perspective of Useful Signal Protection

Hengrui Zhang [1,2,3], Lin Min [1,2,3], Jing Lu [4], Jike Chang [1,5,*], Zhengwei Guo [1,2,3] and Ning Li [1,2,3]

[1] College of Computer and Information Engineering, Henan University, Kaifeng 475004, China; zhr_henu@henu.edu.cn (H.Z.); mlin@henu.edu.cn (L.M.); gzw@henu.edu.cn (Z.G.); hedalining@henu.edu.cn (N.L.)
[2] Henan Engineering Research Center of Intelligent Technology and Application, Henan University, Kaifeng 475004, China
[3] Henan Key Laboratory of Big Data Analysis and Processing, Henan University, Kaifeng 475004, China
[4] Land Satellite Remote Sensing Application Center, Ministry of Natural Resources, Beijing 100048, China; luj@lasac.cn
[5] School of Software, Henan University, Kaifeng 475004, China
* Correspondence: changjike@henu.edu.cn

Abstract: As an open system, synthetic aperture radar (SAR) inevitably receives radio frequency interference (RFI) generated by electromagnetic equipment in the same band. The existence of RFI seriously affects SAR signal processing and image interpretation. In recent years, many algorithms and models related to RFI mitigation have been proposed. However, most of that focus on effectively mitigating the RFI is insufficient to protect the useful signals. This article proposes a mitigation method of RFI with a signal-protected capability. (1) The kurtosis coefficient is used to detect RFI pulse-by-pulse, and the echoes containing RFI are stored in matrix form. (2) The preliminary extraction of RFI is complete by low-rank sparse decomposition of the echo matrix containing RFI. (3) For the secondary separation of RFI, the accurate position of RFI in the preliminary extraction results is located by the fuzzy C-means clustering; then, we separate the RFI and the remaining useful signals again and reconstruct the useful signals to complete the mitigation work. The proposed method can further protect useful signals while effectively removing interference through the secondary separation of RFI. Experimental results based on simulated and measured data verify the performance and potential of the proposed method.

Keywords: synthetic aperture radar; radio frequency interference; interference mitigation; low-rank sparse decomposition

Citation: Zhang, H.; Min, L.; Lu, J.; Chang, J.; Guo, Z.; Li, N. An Improved RFI Mitigation Approach for SAR Based on Low-Rank Sparse Decomposition: From the Perspective of Useful Signal Protection. *Remote Sens.* **2022**, *14*, 3278. https://doi.org/10.3390/rs14143278

Academic Editors: Haipeng Wang, Gang Xu and Lan Du

Received: 30 May 2022
Accepted: 5 July 2022
Published: 7 July 2022

1. Introduction

1.1. Background

Synthetic aperture radar (SAR), as an active microwave sensor, can obtain a high-resolution and a continuous coverage of ground targets all-day/night and all-weather through the combination of wideband signals in range and a synthetic aperture in azimuth. These characteristics make SAR widely used in military reconnaissance, resource exploration, terrain mapping, environmental monitoring, disaster warning and assessment, and other related fields [1–4].

However, SAR is susceptible to various and complex electromagnetic interferences in the operating frequency band as an open broadband system. In general, the signals emitted by other radiation sources in the same frequency band are called radio frequency interference (RFI) to SAR [5–8], which can be divided into narrowband interference (NBI) and wideband interference (WBI) according to the bandwidth of RFI. The existence of RFI will seriously restrict the effect of SAR high-resolution imaging and further affect

the subsequent application of SAR data, such as crop monitoring and natural disaster assessment [9]. It has become a significant research trend to uncover how SAR can survive in this complex electromagnetic environment while maintaining its excellent performance as much as possible [10,11].

With the development of global radio communications, the electromagnetic environment is becoming more and more complex, and RFI cases in SAR systems are becoming more and more common. Domestic and foreign scholars have proposed various RFI mitigation algorithms and models in recent years [12–14]. Among them, the low-rank-sparse model separates interference and useful signals based on RFI's low-rank-sparse characteristics in the transform domain and has a high RFI mitigation accuracy. However, due to the variety of RFI types, the model will inevitably cause the loss of some useful signals while removing RFI, resulting in the loss of details in the SAR image after RFI removal. Therefore, researching mitigation methods of RFI that can consider both the mitigation accuracy of RFI and the adequate protection of useful signals has significant practical application requirements.

1.2. Previous Work

Effectively mitigating RFI in SAR data has always been an important research topic in the SAR field. Since the 1990s, various RFI mitigation methods have been proposed [15], which can be summed up as parametric, non-parametric, and semi-parametric methods [16].

1.2.1. Parametric Methods

The parametric methods complete the RFI mitigation work by establishing the mathematical model of RFI and adjusting the model's parameters. In [17], aiming at the NBI existing in airborne SAR data, the maximum likelihood estimation method was used to mitigate NBI in SAR data by establishing a sine wave model. In [18,19], the NBI model was established based on the narrow-band property of the RFI signal, and a series of RELAX and its improved methods were used to estimate the model parameters, which achieved a satisfactory RFI mitigation effect. In [20], an RFI mitigation method based on the iterative adaptive approach (IAA) and orthogonal subspace projection (OSP) was proposed, which can estimate the RFI power spectrum adaptively and iteratively without a parameter search and model order estimation.

The form of WBI is more complex and diverse than NBI, so it is difficult to establish an accurate parametric model. In [21], IAA was successfully applied to WBI mitigation by improving instantaneous frequency (IF) resolution in short-time Fourier transform (STFT) and filtering WBI based on the OSP method. In [22], a WBI mitigation method combining IF estimation and regularized time–frequency filtering was proposed, which completes the extraction and mitigation of sinusoidally frequency-modulated WBI.

Since it is challenging to establish parametric models of RFI in practical applications, and the mitigation performance of such methods relies on the estimation of model parameters, the application of parametric methods is not sufficiently extensive.

1.2.2. Non-Parametric Methods

The non-parametric method is based on RFI features in the time domain or transform domain for mitigation without establishing a parametric model. In [23], the frequency domain notch filtering (FNF) was simple to implement and had a strong robustness. However, the FNF will lose the useful signal while eliminating the RFI. In order to solve the above problems, a two-step notch method based on a linear prediction model to compensate for the missing spectrum was proposed [24]. In addition, a time domain notch method by constructing a notch filter in the time domain and using the IAA to recover missing signals was proposed [25], which improved the accuracy of interference mitigation and reduced the loss of useful signals.

The adaptive filtering method separates useful signals from interference by constructing an adaptive filter. In [26], an adaptive spectrum line enhancer was proposed, which can improve the mitigation of time varying NBI. An adaptive Wiener filter was proposed in [27], which achieved better performance than the LMS adaptive filter.

The matrix decomposition-based methods, such as eigen-subspace projection (ESP) [28], independent component analysis [29], complex empirical mode decomposition [30], and independent subspace analysis [31], decompose the echo data into useful signal components and RFI components, thereby realizing the mitigation of RFI. The matrix decomposition-based methods can effectively mitigate the NBI and WBI, but these methods are ineffective in the case of weak RFI.

Different from the above methods that are mainly applied to SAR level-0 products (raw data), the sub-band spectrum cancellation (SSC) method [32] and the block subspace filtering (BSF) method [33] are non-parametric methods for level-1 products (single look complex data). The SSC method is based on the assumption that the distance spectrum is strictly symmetric. Otherwise, the RFI mitigation performance would drop significantly. BSF is based on the assumption that the RFI-free SAR image conforms to the Gaussian distribution, and the intensity of RFI is higher than the useful signal to ensure mitigation accuracy. In [34], a mitigation method of RFI for SAR images with joint change detection and sub-band spectrum cancellation was proposed, effectively preserving target information while mitigating interference.

1.2.3. Semi-Parametric Methods

With the development of the low-rank sparse decomposition (LRSD) algorithm, robust principal component analysis (RPCA) has been used in SAR signals for various applications, such as clutter suppression and moving target detection by separating moving and stationary targets in SAR images [35–39]. In recent years, the theory of LRSD has been successfully applied to mitigate RFI in SAR data. This method converts complex signal separation problems into hyperparameter optimization problems and forms a semi-parametric mitigation method of RFI. In [40], the concept of semi-parametric interference mitigation was proposed, which completed the mitigation of NBI by solving the sparse reconstruction optimization problem. In [41], the sparse reconstruction algorithm was extended to WBI, providing a new idea for the extended application of these methods. In [42–44], a series of low-rank-sparse decomposition models were proposed, further improving the related theories. In [45] a dictionary-based SAR RFI-suppression method under the framework of RPCA was proposed. In [46], a two-dimensional RFI mitigation method was proposed and applied to simulated and measured data successfully. In [47], a graph Laplacian clustering algorithm was proposed to mitigate RFI. In [48], a mitigation algorithm of RFI that combines low-rank and double-sparse features was proposed based on RFI's low-rank and sparse features.

In general, the semi-parametric approaches utilize optimized models to constrain and separate the RFI. However, due to the various RFI types, these models will inevitably cause the loss of some useful signals while removing RFI, resulting in the loss of details in the SAR image.

Moreover, with the development of deep learning methods, intelligent learning methods have become an emerging trend in signal processing. Methods based on neural networks, especially combined with RPCA and applied to RFI mitigation in SAR data, have shown superior performance and potential. In [49], a method to mitigate RFI using a special type of convolutional neural network, the U-Net, was proposed. In [50], a mitigation algorithm of NBI and WBI based on the deep residual network (ResNet) was proposed. In [51], a hybrid model-constrained deep learning approach for RFI extraction and mitigation by fusing the classical model-based and advanced data-driven method was proposed. However, these methods are inherently black box, lacking a certain degree of interpretability, and since their performance relies on access to large amounts of data and computational resources, this limits their applicability to scenarios with limited samples.

1.3. Solution and Contributions of This Article

Given the above problems, this study makes full use of the low-rank characteristics of RFI in the range frequency domain and proposes a mitigation method of RFI with a signal-protected capability. First, the kurtosis coefficient method is used to detect RFI pulse-by-pulse in the range frequency domain, and the echoes containing RFI are stored in the form of a matrix. Second, the RFI is preliminary extracted, which is completed by the LRSD of the echo matrix containing RFI; after decomposition, the low-rank matrix representing RFIs can be preliminary separated. Lastly, for the secondary separation of RFI, we use the fuzzy C-means (FCM) clustering algorithm to pinpoint the RFI in the preliminary extraction results, then, we separate the RFI from the remaining useful signal in the low-rank matrix again and reconstruct the useful signal to complete the mitigation. The proposal can further protect useful signals while removing interference through the secondary separation of RFI effectively. Experimental results based on simulated and measured data verify the performance and potential of the proposed method.

The main contributions of this article are summarized as follows:

1. An idea of implementing secondary separation for RFI is proposed, which can solve the insufficient protection of useful signals in traditional mitigation methods of RFI. By separating the extraction results of RFI again, the loss of useful signals can be effectively reduced. In particular, this idea of secondary separation can be extended to other mitigation methods of RFI, which provides a new perspective of RFI mitigation in SAR data;
2. This study proposes a mitigation approach for RFI with a signal protection capability based on the low-rank property of RFI in the range frequency domain. Specifically, the method includes three steps: the detection, extraction, and secondary separation of RFI. Compared with traditional methods, this proposal pays more attention to the preservation of SAR image details while effectively detecting and mitigating RFI, avoiding the situation that the interpretation of SAR images is more difficult due to excessive loss of useful signals after RFI mitigation.

Theoretical discussions are validated through extensive experiments. Specifically, in experiments with simulated data, the mitigation effect and useful signal protection capability of the proposed method under different bandwidths of RFI and different SINRs are discussed. Experiments with the measured data verify the effectiveness and superiority of the proposed method.

1.4. Organization of This Article

The remainder of this article is organized as follows. Section 2 introduces the geometric and signal models and analyzes the sparse and statistical characteristics of RFI in the range frequency domain. Section 3 shows the detailed workflow of the RFI mitigation method proposed in this article. Section 4 gives the experimental results and performance analysis of the method. Lastly, Section 5 concludes this article and discusses the further application of the method.

2. Problem Formulation

2.1. Geometric Model of RFI

Various electromagnetic devices operating in the same frequency band as SAR systems are major sources of RFI. In recent years, many RFI cases have been observed in spaceborne and airborne SAR data, among which the main sources are not only space-based sources such as airborne radars and co-frequency satellites but also ground-based sources such as ground base stations and ground-based radars. In general, the spatial relationship between the RFI sources and the irradiated area of the spaceborne SAR beam is shown in Figure 1. For ground-based sources, RFI is usually received in the form of direct waves by the main or side lobes of the SAR. For space-based sources, RFI is usually received by the SAR in the form of direct or scattered waves.

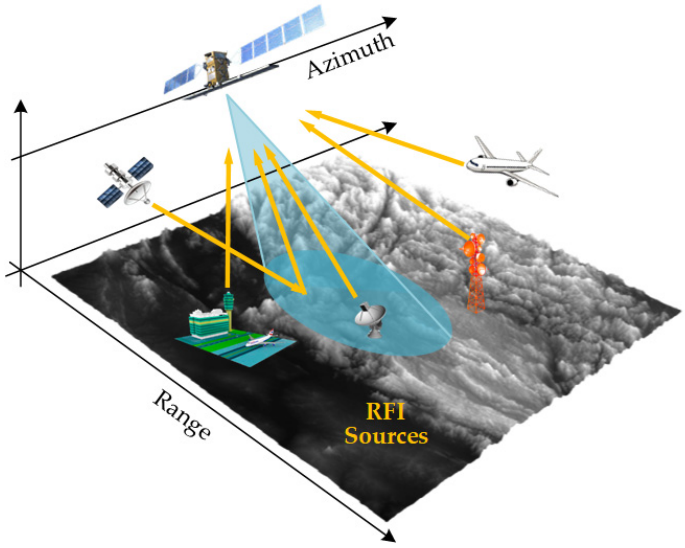

Figure 1. Common sources and geometric model of RFI.

2.2. Signal Model of RFI

When the SAR system is working, the raw signal is usually superimposed into the azimuth (i.e., slow time) and the range (i.e., fast time) domain. Since the RFI signal is independent of the SAR echo signal, in each azimuth echo [25], the SAR echo containing RFI can be expressed as

$$S(\tau,\eta) = X(\tau,\eta) + I(\tau,\eta) + N(\tau,\eta) \tag{1}$$

where $X(\tau,\eta)$, $I(\tau,\eta)$, and $N(\tau,\eta)$ represent the useful signal, RFI, and system noise, respectively. τ and η represent the range fast time and the azimuth slow time, respectively.

Although there are many different forms of RFI, in general, RFI is considered to be a linear combination of multiple single frequencies caused by radiating sources. According to its bandwidth, it can be divided into two categories: NBI and WBI. As mentioned in [15], NBI can be regarded as the superposition of a series of sinusoidal signals, and its model can be expressed as

$$I_{NBI}(\tau,\eta) = \sum_{n=1}^{N} A_n(\eta) exp(2j\pi f_n \tau + \varphi_n) \tag{2}$$

where N represents the number of interference signals. $A_n(\eta)$, f_n, and φ_n represent the amplitude, frequency, and phase of the nth interference signal, respectively. NBI generally does not have a complex frequency modulation, and often appears in the form of bright lines in the image.

In contrast, WBI has a larger bandwidth and a more complex frequency modulation, occupying more frequency cells in the range frequency domain. Typically, WBI can be modeled as linear frequency modulation (LFM) and sinusoidal frequency modulation (SFM) [25]. Its signal model can be expressed as

$$I_{WBI}(\tau,\eta) = \sum_{n=1}^{N} A_n(\eta) exp(j\phi) \tag{3}$$

where the phase term ϕ is divided into two modulation terms, ϕ_{LFM} and ϕ_{SFM}, which represent LFM and SFM, respectively. The specific form is

$$\phi_{LFM} = 2\pi f_n \tau + \pi K_n \tau^2 \tag{4}$$

$$\phi_{SFM} = \beta_n sin(2\pi f_n \tau + \varphi_n) \tag{5}$$

where K_n represents the chirp rate of the nth WBI signal, and β_n represents the modulation factor.

2.3. Low-Rank Sparse Model

The linear reversibility of the fast Fourier transform (FFT) ensures that this transform does not affect the linear superposition characteristics of the SAR echo. Therefore, according to (5), the SAR echo data can be expressed as

$$S(f_\tau, \eta) = X(f_\tau, \eta) + I(f_\tau, \eta) + N(f_\tau, \eta) \tag{6}$$

where f_τ represents the range frequency cells after FFT.

The RFI in the range frequency domain has a relatively stable frequency in the slow time direction, and its amplitude appears as some parallel straight lines, as shown in Figure 2a. It is clear that RFI has low-rank properties in the slow time direction. For further verification, the eigenvalue decomposition of Figure 2a is performed, and the corresponding results are shown in Figure 2b. The eigenvalues reflect the energy of different components in the SAR echo and the structural redundancy of the matrix. As can be observed, only a few large eigenvalues are related to RFI, which further illustrates the low-rank feature of RFI in the range frequency domain.

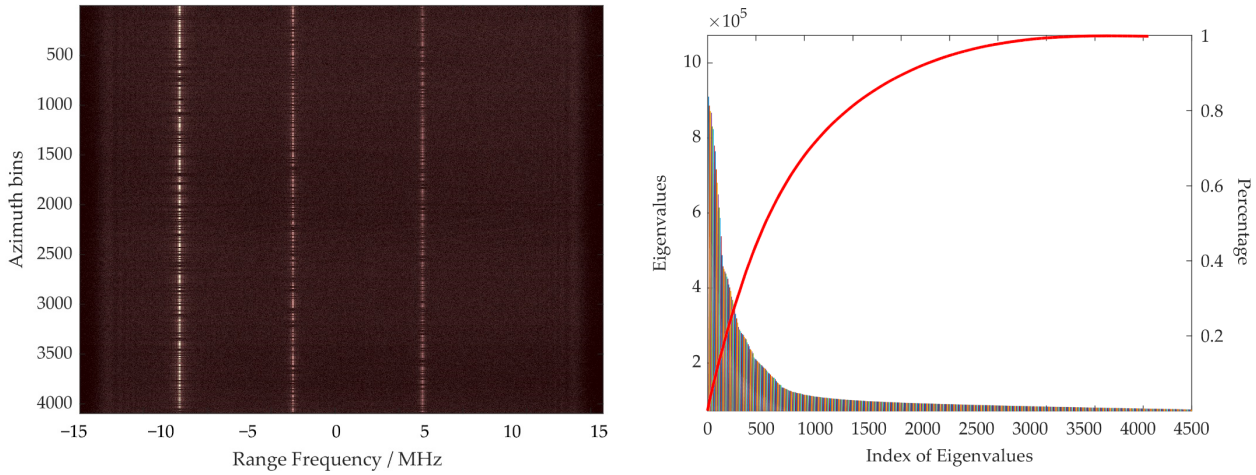

(**a**) (**b**)

Figure 2. Structural analysis of RFI in range frequency domain: (**a**) spectrogram of SAR echoes contaminated by RFI; (**b**) Eigenvalue sequences and analysis corresponding to (**a**).

According to the low-rank characteristic of RFI in the frequency domain, RFI can be initially extracted by solving the following LRSD problem.

$$\begin{aligned} \underset{\mathbf{I},\mathbf{X}}{min} \quad & rank(\mathbf{I}) + \lambda \|\mathbf{X}\|_0 \\ s.t. \quad & \mathbf{S} = \mathbf{I} + \mathbf{X} \end{aligned} \tag{7}$$

where $rank(\cdot)$ represents the rank of the matrix, $\|\cdot\|_0$ represents the ℓ_0 norm of the matrix, that is, the number of non-zero elements in the matrix, and $\lambda > 0$ is a compromise factor.

The rank and ℓ_0 norm of matrices can be convexly relaxed, providing a way to solve the above issues. Since the kernel norm of the matrix is the convex envelope of the rank, and the ℓ_1 norm of the matrix is the optimal convex approximation of ℓ_0, (7) can be relaxed as the following convex optimization problem.

$$\begin{aligned} \underset{\mathbf{I},\mathbf{X}}{min} \quad & \|\mathbf{I}\|_* + \lambda \|\mathbf{X}\|_1 \\ s.t. \quad & \mathbf{S} = \mathbf{I} + \mathbf{X} \end{aligned} \tag{8}$$

where $\|\cdot\|_*$ is the kernel norm that can represent the sum of the singular values of the matrix, $\|\cdot\|_1$ represents the ℓ_1 norm of the matrix, that is, the sum of the absolute values of each element in the matrix, as mentioned in [12], the compromise factor λ is set as:

$$\lambda = \frac{1}{\sqrt{\max(m,n)}} \tag{9}$$

where m and n represent the number of rows and columns of matrix S, respectively.

2.4. Statistical Model

Generally speaking, under the assumption of complex Gaussian distribution of a SAR echo without RFI, the real and imaginary parts of its range frequency domain spectrogram obey Gaussian distribution. When there is RFI in the echo, the histogram will deviate from the Gaussian distribution and be more concentrated in the low-amplitude region, resulting in sharper peaks on the left and tails on the right.

Figure 3a,b sequentially shows the frequency amplitude images of RFI-free and RFI-containing echoes, and Figure 3c shows the frequency amplitude images of the RFI extracted by LRSD. It can be clearly observed that some useful signals remain in Figure 3c. The amplitude histograms of Figure 3a–c are separately counted for further analysis, as shown in Figure 3d–f. It can be seen that Figure 3d–f all obey the Rayleigh distribution. Figure 3e has a sharper left peak than Figure 3d, while Figure 3f has the sharpest left peak, and there are remaining useful signals in the right tail.

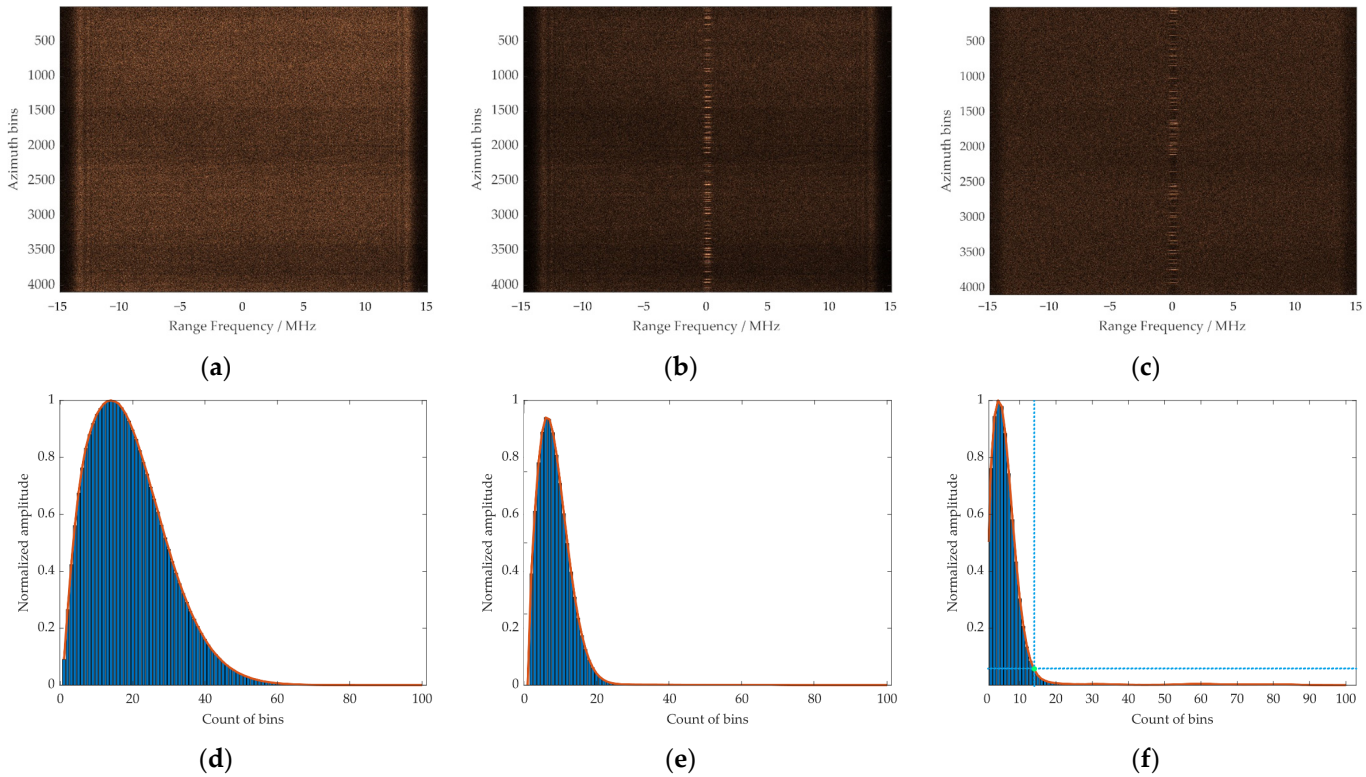

Figure 3. Statistical analysis of SAR range frequency spectrogram: (**a**) RFI-free signal; (**b**) RFI-containing signal; (**c**) Extraction of RFI; and (**d**–**f**) The amplitude histograms correspond to (**a**–**c**), respectively.

Through the above analysis, this study performs LRSD based on the low-rank characteristic of RFI to realize the extraction of RFI. On the basis of RFI extraction, a binary masking matrix is generated for the low-rank matrix, so as to complete the secondary separation of RFI.

3. Methodology

In order to solve the problem of RFI detection and mitigation in SAR data, a mitigation method of RFI with signal protection capability is proposed. Specifically, the method includes three steps: RFI detection based on kurtosis, RFI extraction based on LRSD, and RFI secondary separation based on binary masking. The proposal can detect and mitigate RFI robustly while protecting useful SAR signals and effectively reducing the loss of details in SAR images. The specific flow chart is shown in Figure 4.

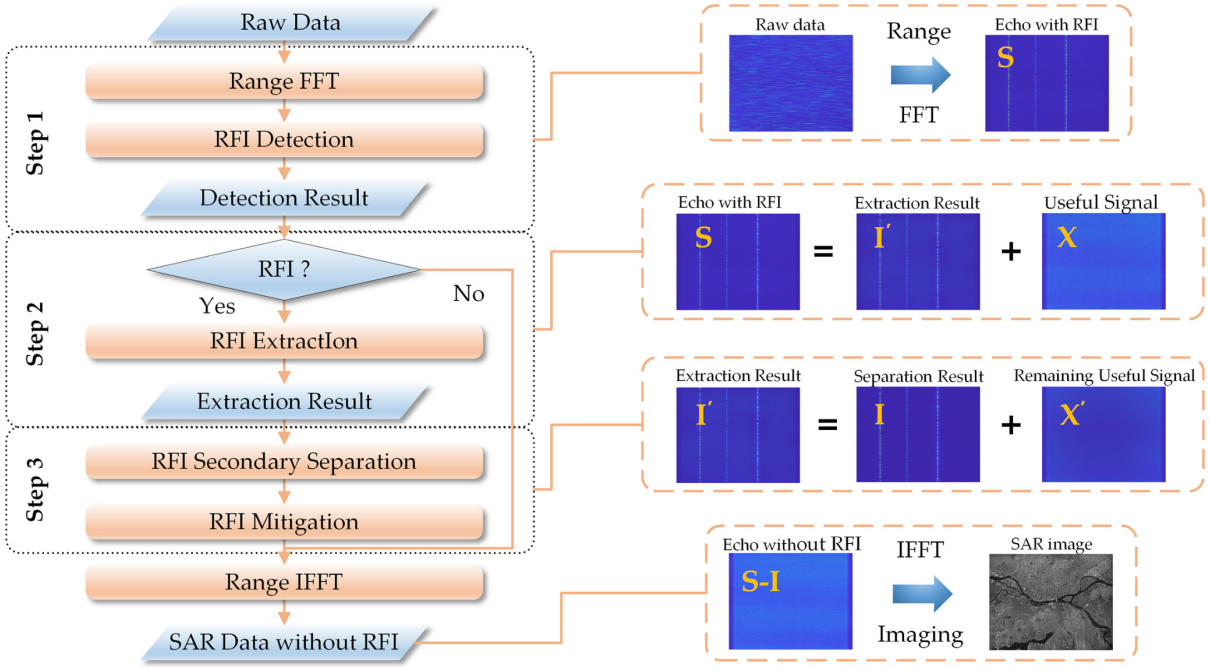

Figure 4. Flow chart of the proposed method.

3.1. RFI Detection Based on Kurtosis

In order to accurately and efficiently mitigate the RFI and protect the useful signal as much as possible, it is necessary to perform detection of RFI pulse-by-pulse. Unlike the traditional mitigation method, which needs to detect the position of RFI in the frequency domain accurately, the method proposed in this study only needs to distinguish between the RFI-containing echo and the useful signal. Considering the difference in statistical characteristics between the SAR signal and RFI, the presence of RFI can be quickly detected by calculating the kurtosis of the frequency domain echoes [52].

Assuming that S is a random variable, the mean is u, and σ is the standard deviation, the kurtosis can be defined as:

$$K(S) = \frac{E[S-u]^4}{\sigma^4} = \frac{\frac{1}{n}\sum_{i=1}^{n}(s_i-\bar{s})^4}{\left(\frac{1}{n}\sum_{i=1}^{n}(s_i-\bar{s})^2\right)^2} \tag{10}$$

where $E[\cdot]$ denotes the expectation operator. Kurtosis characterizes the steepness of distribution, which is usually a statistic relative to a normal distribution. If the kurtosis is greater than 3, the sample has a steep distribution, and conversely, it has a flat distribution.

It is supposed that N_r and N_a denote the number of samples for range and azimuth, respectively. By calculating the kurtosis of each echo in a pulse-by-pulse manner, a sequence of kurtosis values can be obtained, which can be expressed as

$$\Phi(i) = [K_1, K_2, \ldots, K_{N_r}] \tag{11}$$

The robust K-means algorithm [53] is used to classify $\Phi(i)$ into two categories, one of which indicates the presence of RFI and the other indicates the absence. The operation of threshold segmentation can be expressed as

$$\overline{\Phi}(i) = \begin{cases} 0, & \Phi(i) < \alpha, \quad \Rightarrow Without\ RFI \\ 1, & \Phi(i) \geq \alpha, \quad \Rightarrow With\ RFI \end{cases} \tag{12}$$

where $\overline{\Phi}(i)$ is the detection result, α is the threshold, and constants 1 and 0 indicate the presence and absence of RFI, respectively.

3.2. Extraction of RFI Based on LRSD

After the detection work, it is necessary to perform LRSD on the RFI-containing echo in the frequency domain to complete RFI extraction, which can be transformed to obtain the optimal solution to the convex problem (8) based on the analysis in Section 2. The alternating direction multiplier method (ADMM) adopts the idea of divide and conquer, which can be applied to the solution of large-scale optimization problems and obtain the optimal solution of the problem. The augmented Lagrangian function is constructed as follows.

$$L(\mathbf{I}, \mathbf{X}, \mathbf{Y}, \mu) = \|\mathbf{I}\|_* + \lambda\|\mathbf{X}\|_1 - \langle \mathbf{Y}, \mathbf{I} + \mathbf{X} - \mathbf{S} \rangle + \frac{\mu}{2}\|\mathbf{I} + \mathbf{X} - \mathbf{S}\|_F \tag{13}$$

where μ is the penalty factor, $\mathbf{Y}$ is the Lagrange multiplier, $\langle \cdot \rangle$ represents the matrix inner product, and $\| \cdot \|_F$ represents the Frobenius norm. When $\mathbf{Y} = \mathbf{Y}_k$, $\mu = \mu_k$, use the ADMM method to solve the block optimization problem.

$$\min_{\mathbf{I},\mathbf{X}} \quad L(\mathbf{I}, \mathbf{X}, \mathbf{Y}_k, \mu_k) \tag{14}$$

First, fix the variables $\mathbf{X}$ and $\mathbf{Y}$, and the operation of updating the variable $\mathbf{I}$ is as follows.

$$\begin{aligned} \mathbf{I}_{k+1} &= arg\ \min_{\mathbf{I}} L(\mathbf{I}, \mathbf{X}_{k+1}, \mathbf{Y}_k, \mu_k) \\ &= arg\ \min_{\mathbf{I}} \| \mathbf{I} \|_* - \langle \mathbf{Y}_k, \mathbf{I} + \mathbf{X}_{k+1} - \mathbf{S} \rangle + \tfrac{\mu_k}{2} \| \mathbf{I} + \mathbf{X}_{k+1} - \mathbf{S} \|_F \\ &= arg\ \min_{\mathbf{I}} \| \mathbf{I} \|_* + \tfrac{\mu_k}{2} \| \mathbf{I} - \left(\mathbf{S} - \mathbf{X}_{k+1} + \tfrac{\mathbf{Y}_k}{\mu_k} \right) \|_F \\ &= G_{\frac{1}{\mu_k}} \left(\mathbf{S} - \mathbf{X}_{k+1} + \tfrac{\mathbf{Y}_k}{\mu_k} \right) \end{aligned} \tag{15}$$

where $G_{\frac{1}{\mu_k}}(\cdot)$ is the shrinkage operator of singular threshold, and the specific operation can be described as:

$$\mathbf{W}' = G_{\frac{1}{\mu_k}}(\mathbf{W}) = \begin{cases} [\mathbf{U}, \mathbf{\Sigma}, \mathbf{V}] = svd(\mathbf{W}) \\ \mathbf{\Sigma} = sgn(\mathbf{\Sigma}) \cdot * max(abs(\mathbf{\Sigma}) - \frac{1}{\mu_k}, 0) \\ \mathbf{W}' = \mathbf{U} * \mathbf{\Sigma} * \mathbf{V}^H \end{cases} \tag{16}$$

where $[\mathbf{U}, \mathbf{\Sigma}, \mathbf{V}] = svd(\mathbf{W})$ is the singular value decomposition of $\mathbf{W}$.

Then, fix the variables $\mathbf{I}$ and $\mathbf{Y}$, and the operation of updating the variable $\mathbf{X}$ is as follows.

$$\begin{aligned} \mathbf{X}_{k+1} &= arg\ \min_{\mathbf{X}} L(\mathbf{I}_{k+1}, \mathbf{X}, \mathbf{Y}_k, \mu_k) \\ &= arg\ \min_{\mathbf{X}} \lambda \| \mathbf{X} \|_1 - \langle \mathbf{Y}_k, \mathbf{I}_{k+1} + \mathbf{X} - \mathbf{S} \rangle + \tfrac{\mu_k}{2} \| \mathbf{I}_{k+1} + \mathbf{X} - \mathbf{S} \|_F \\ &= arg\ \min_{\mathbf{X}} \lambda \| \mathbf{X} \|_1 + \tfrac{\mu_k}{2} \| \mathbf{X} - \left(\mathbf{S} - \mathbf{I}_{k+1} + \tfrac{\mathbf{Y}_k}{\mu_k} \right) \|_F \\ &= F_{\frac{\lambda}{\mu_k}} \left(\mathbf{S} - \mathbf{I}_{k+1} + \tfrac{\mathbf{Y}_k}{\mu_k} \right) \end{aligned} \tag{17}$$

where $F_{\frac{\lambda}{\mu_k}}(\cdot)$ is the shrinkage operator of soft threshold, and the specific operation can be described as:

$$F_{\frac{\lambda}{\mu_k}}(\mathbf{W}) = sign(\mathbf{W}) \cdot * \, max(abs(\mathbf{W}) - \frac{1}{\mu_k}, 0) \tag{18}$$

when $\mathbf{I} = \mathbf{I}_{k+1}$, $\mathbf{S} = \mathbf{S}_{k+1}$, the update formula of matrix $\mathbf{Y}$ is

$$\mathbf{Y}_{k+1} = \mathbf{Y}_k - \mu_k(\mathbf{I}_{k+1} + \mathbf{S}_{k+1} - \mathbf{R}) \tag{19}$$

the penalty factor μ_k can be updated as follows.

$$\mu_{k+1} = \begin{cases} \rho\mu_k & \frac{\mu_k \|\mathbf{X}_{k+1} - \mathbf{X}_k\|_F}{\|\mathbf{S}\|_F} < \varepsilon \\ \mu_k & otherwise \end{cases} \tag{20}$$

therefore, the optimization problem of (8) can be solved iteratively by (15), (17), and (19). It can provide extraction results of RFI until convergence, that is

$$I'(f_\tau, \eta) = \mathbf{I}_k \tag{21}$$

3.3. Secondary Separation of RFI

Since there are various forms of RFI in the actual scene, and the result of LRSD is an approximate solution to the convex optimization problem, some useful signals will inevitably remain in the extracted RFI matrix. It can be expressed as

$$I'(f_\tau, \eta) = I(f_\tau, \eta) + X'(f_\tau, \eta) \tag{22}$$

where $I(f_\tau, \eta)$ is the RFI actually present in the SAR echo and $X'(f_\tau, \eta)$ represents the remaining useful signal.

In order to further reduce the loss of useful signals after RFI mitigation, this study proposes a secondary separation of RFI, the process is shown in Figure 5.

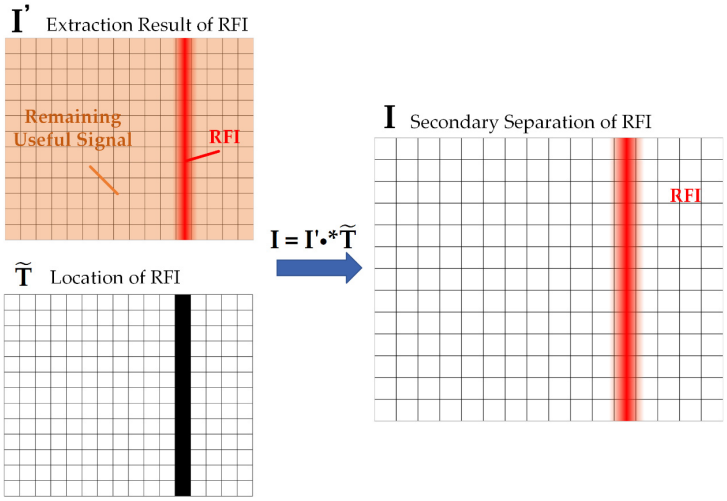

Figure 5. The secondary separation process of RFI.

The secondary separation of RFI is done by using the FCM algorithm to generate a binary masking matrix $\tilde{\mathbf{T}}(f_\tau, \eta)$ from the extraction result of RFI. Then, the secondary separation can be expressed as

$$I(f_\tau, \eta) = I'(f_\tau, \eta) * \tilde{\mathbf{T}} \tag{23}$$

Finally, the useful signal can be reconstructed by removing the RFI, which can be expressed as

$$X_{total}(f_\tau, \eta) = S(f_\tau, \eta) - I(f_\tau, \eta) \tag{24}$$

Through the above detection, extraction, and secondary separation of RFI, the SAR echo without RFI can be obtained. The specific steps of the proposed method are summarized in Algorithm 1, and the detailed performance will be presented in the following subsection.

Algorithm 1 Extraction and Secondary Separation of RFI

Input: $\mathbf{S} = S(f_\tau, \eta)$, $\lambda > 0$, $\mu_0 > 0$, $\rho > 1$, $\delta > 0$
Initialization: $\mathbf{I}_0 = 0$, $\mathbf{X}_0 = 0$, $\mathbf{Y}_0 = \frac{\mathbf{S}}{max\left(\|\mathbf{S}\|_2, \sqrt{mn}\|\mathbf{S}\|_\infty\right)}$, $k = 0$
While $\|\mathbf{S} - \mathbf{I}_{k+1} + \mathbf{X}_{k+1}\|_F^2 / \|\mathbf{I}\|_F^2 > \delta$ do
Low rank matrix: $\mathbf{I}_{k+1} = G_{\frac{1}{\mu_k}}\left(\mathbf{S} - \mathbf{X}_{k+1} + \frac{\mathbf{Y}_k}{\mu_k}\right)$
Sparse matrix: $\mathbf{X}_{k+1} = F_{\frac{\lambda}{\mu_k}}\left(\mathbf{S} - \mathbf{I}_{k+1} + \frac{\mathbf{Y}_k}{\mu_k}\right)$
Update variable $\mathbf{Y}$: $\mathbf{Y}_{k+1} = \mathbf{Y}_k - \mu_k(\mathbf{I}_{k+1} + \mathbf{X}_{k+1} - \mathbf{S})$
Update penalty factor μ: $\mu_{k+1} = \begin{cases} \rho\mu_k & \frac{\mu_k\|\mathbf{X}_{k+1} - \mathbf{X}_k\|_F}{\|\mathbf{S}\|_F} < \varepsilon \\ \mu_k & otherwise \end{cases}$
$k = k + 1$
End while
Extraction of RFI: $I'(f_\tau, \eta) = \mathbf{I}_k$
Generate binary masking matrix: $\tilde{\mathbf{T}}(f_\tau, \eta)$
RFI secondary separation: $I(f_\tau, \eta) = I'(f_\tau, \eta) \cdot * \tilde{\mathbf{T}}$
Remove RFI: $X_{total}(f_\tau, \eta) = S(f_\tau, \eta) - I(f_\tau, \eta)$
Output: $I(f_\tau, \eta)$, $X_{total}(f_\tau, \eta)$

4. Experimental Results and Discussion

Extensive experiments are performed in this section using simulated SAR data and Sentinel-1 level-0 raw data. Specifically, based on real SAR data and simulated RFI, the mitigation performance of the proposed method is quantitatively analyzed by comparing the root mean square error (RMSE) under different signal-to-interference and noise ratios (SINR) and different RFI bandwidths. Experiments based on measured SAR data verify the effectiveness of the method, and the mitigation performance is evaluated by calculating the gray level entropy and average gradient of the SAR image after RFI mitigation.

4.1. Experimental Results Based on Simulated SAR Data

4.1.1. On the Performance of RFI Mitigation for Different SINR Cases

Simulated experiments based on different SINRs are used to verify the RFI mitigation performance of the proposed method. Furthermore, by comparing the proposal with ESP [28], RPCA [8], and complex tensor RPCA (CT-RPCA) [44] methods, the potential of the proposed method for useful signal protection is further verified. Table 1 summarizes the main system parameters of the simulation.

The experimental results of the proposed method compared with ESP, RPCA, and CT-RPCA are shown in Figure 6. It can be seen from the first row that the RFI under different SINRs has different degrees of contamination to the SAR image. At the SINR of –30, the artifacts caused by RFI significantly suppress scene information. The following four rows are the RFI mitigation results after using ESP, RPCA, CT-RPCA, and the proposed method. As can be seen from Figure 6, all four methods can effectively mitigate RFI under different SINR conditions but have different performances in the protection of useful signals. The magnified region marked with a red box in Figure 6 is the region of interest (ROI), as shown in Figure 7. It can be seen from Figure 7a–d that there are abnormal sidelobe effects on the point targets of the image after RFI suppression using the ESP method, which is due to the loss of useful signals caused by the method over-penalizing the eigenvalues when reconstructing the RFI. Figure 7e–l show the corresponding ROIs after using the RPCA and

CT-RPCA methods. Since these two methods do not further separate the remaining useful signals after the low-rank and sparse decomposition of the SAR signal, the high sidelobe phenomenon still exists to varying degrees. Figure 7m–p show the corresponding ROIs after the proposed method mitigates RFI, and it can be seen that the high sidelobe effect of the point target is no longer present. This indicates that this method can further protect the useful signal while effectively removing RFI.

Table 1. Main parameters of measured SAR data and simulated RFI.

Parameters	Values
Carrier frequency	5.300 GHz
Sampling frequency	32.317 MHz
Efficient velocity	7000 m/s
Slant range	988,647 m
PRF	1256.98 Hz
Pulse width	41.74 μm
Pulse bandwidth	30 MHz
Carrier frequency of RFI	5.305 GHz
Bandwidth of RFI	1 MHz

To quantitatively evaluate the performance of the interference mitigation method, the RMSE was selected as the evaluation index to evaluate the mitigation results in the experiment. RMSE is defined as

$$RMSE(\mathbf{X}, \mathbf{S}) = \frac{\|\mathbf{S} - \mathbf{X}\|_F}{\|\mathbf{S}\|_F} \tag{25}$$

RMSE describes the normalized difference between the original and recovered SAR data. The smaller the RMSE, the better the mitigation performance. Table 2 summarizes the RMSE comparison results of ESP, RPCA, CT-RPCA, and the proposed method under different SINR conditions. The results show that the RMSE of the proposed method is lower under different SINR conditions, which means that the proposed method has a more prominent signal protection performance while mitigating RFI.

Table 2. Evaluation metrics for the four methods in the different SINR cases.

Metric \ Method		ESP	RPCA	CT-RPCA	Proposed Method
RMSE	SINR = 0 dB	0.1851	0.1926	**0.1648**	0.1695
	SINR = −10 dB	0.2295	0.2198	0.2221	**0.2126**
	SINR = −20 dB	0.2691	0.2797	0.2536	**0.2450**
	SINR = −30 dB	0.2926	0.3050	0.2878	**0.2816**

The best results in each metric are highlighted in bold.

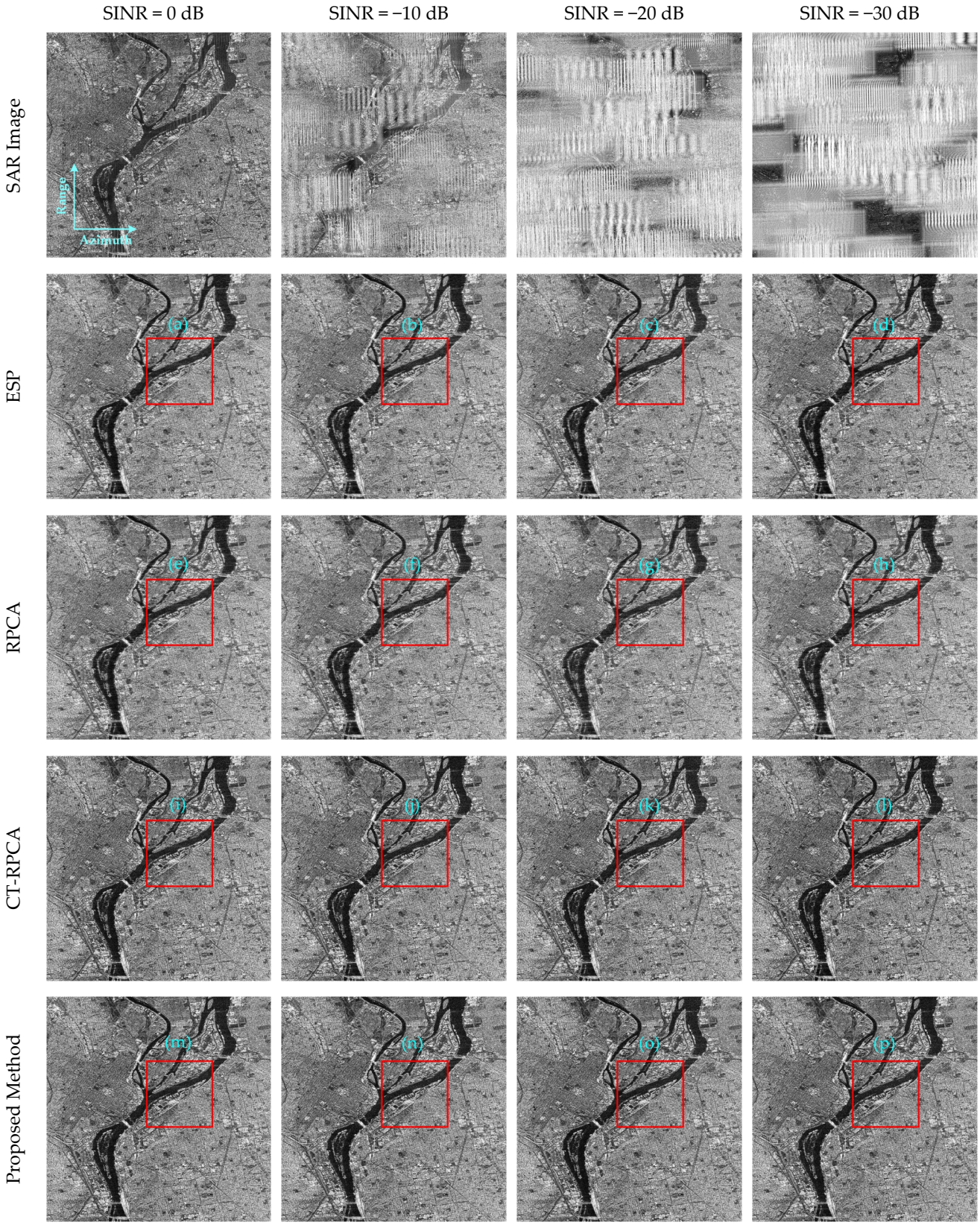

Figure 6. RFI mitigation performance for the ESP, RPCA, CT-RPCA, and proposed approach under different SINRs. (**a**–**p**) ROIs for RFI mitigation results of different methods.

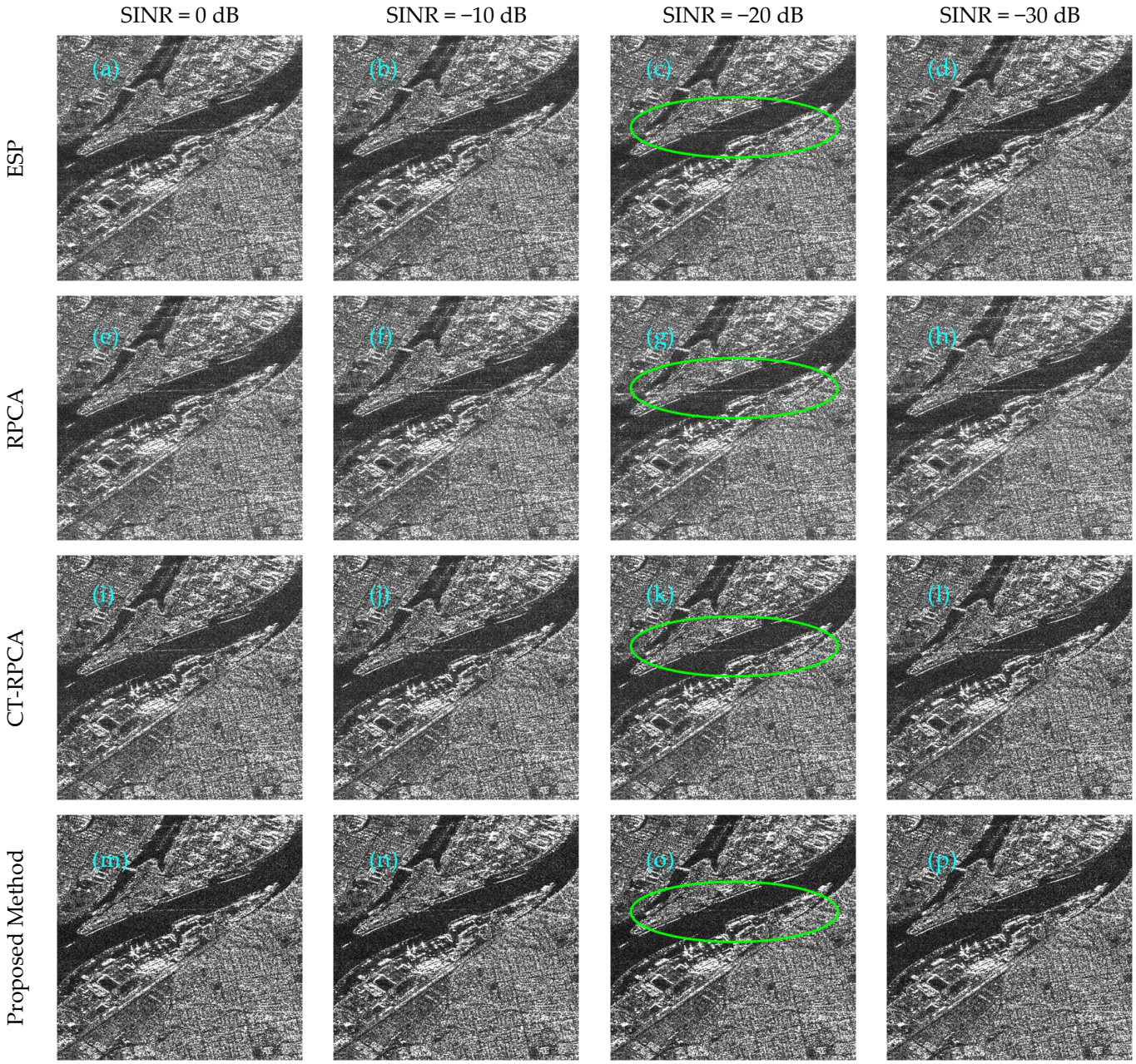

Figure 7. ROIs in Figure 6. (**a**–**d**) Mitigation results for the ESP method. (**e**–**h**) Mitigation results for the RPCA method. (**i**–**l**) Mitigation results for the CT-RPCA method. (**m**–**p**) Mitigation results for the proposed approach.

4.1.2. On the Performance of Mitigation for Different Bandwidths of RFI

Simulation experiments were used to explore the proposed method's mitigation performance under different RFI bandwidths and compared with ESP, RPCA, and CT-RPCA methods. The experimental results are shown in Figure 8. From the first row, it can be seen that RFI with different bandwidths has different degrees of influence on the SAR image. When the bandwidth of RFI is 2 MHz, the four methods can effectively mitigate RFI. While the details in the SAR images using the proposed method are clearer, indicating that it is more effective in protecting useful signals, which is verified by subsequent quantitative analysis. When the bandwidth is increased to 4 MHz, the high sidelobe effect caused by the ESP and RPCA methods is more obvious in the SAR images, and the proposed method

still shows excellent performance. When the bandwidth is increased to 6 MHz, the RFI mitigation performance of the proposed method degrades.

The magnified view of the ROI marked by the red box in Figure 8 is shown in Figure 9. It is evident from Figure 9a–c that the loss of useful signal caused by ESP methods becomes more severe as the RFI bandwidth increases. Figure 9d–i show the corresponding ROIs for the RPCA and CT-RPCA method, and it can be found that when the RFI bandwidth is increased from 2 M to 6 M, the high sidelobe effect caused by the loss of useful signal still exists since these two methods only rely on LRSD to extract the RFI. Figure 9j–l shows the corresponding ROI of the proposed method. It can be seen that when the bandwidth of the RFI exceeds 4 M, although the interference mitigation effect of the method begins to decline, the useful signal can still be effectively protected.

Table 3 summarizes the RMSE comparison results of ESP, RPCA, CT-RPCA, and the proposed method under different RFI bandwidths.

Table 3. Evaluation metrics for the four methods in the different bandwidths of RFI.

Metric \ Method		ESP	RPCA	CT-RPCA	Proposed Method
RMSE	Bandwidth = 2 MHz	0.1868	0.2202	0.1853	**0.1819**
	Bandwidth = 4 MHz	0.2419	0.2377	0.2260	**0.2138**
	Bandwidth = 6 MHz	0.3477	0.3534	**0.3305**	0.3340

The best results in each metric are highlighted in bold.

4.2. Experimental Results Based on Measured Data

Experiments are implemented using Sentinel-1 (TOPS mode) level-0 raw data to verify the method's effectiveness. The performance of different methods for RFI mitigation was evaluated by calculating the gray level entropy and average gradient of SAR images after RFI mitigation.

4.2.1. Experimental Data Description

Figure 10 shows a pseudo color image of the measured Sentinel-1 level-0 raw data. The data were acquired on 12 February 2020. As shown in Figure 10a, the SAR image is heavily contaminated by RFI due to multiple potential sources of interference in the illuminated area. The RFI-corrupted burst is shown in Figure 10b. It can be observed that the artifacts generated by RFI are all over the image.

4.2.2. Experimental Results Based on Spaceborne SAR Data

Figure 11 shows the RFI mitigation results for Sentinel-1 Level-0 raw data. Figure 11a–d show the RFI mitigation results for ESP, RPCA, CT-RPCA, and the proposed method. Figure 11e–h show the ROIs in Figure 11a–d. It is obvious that after using the ESP method, the artifacts generated by RFI in the image have been effectively removed, while the image quality is significantly degraded due to the raised sidelobes of the strongly scattering targets. When using the RPCA and CT-RPCA methods, the image still has certain sidelobe effects due to the loss of part of the useful signal during RFI mitigation. While the proposed method pays more attention to signal protection, it can avoid the loss of image details after RFI mitigation.

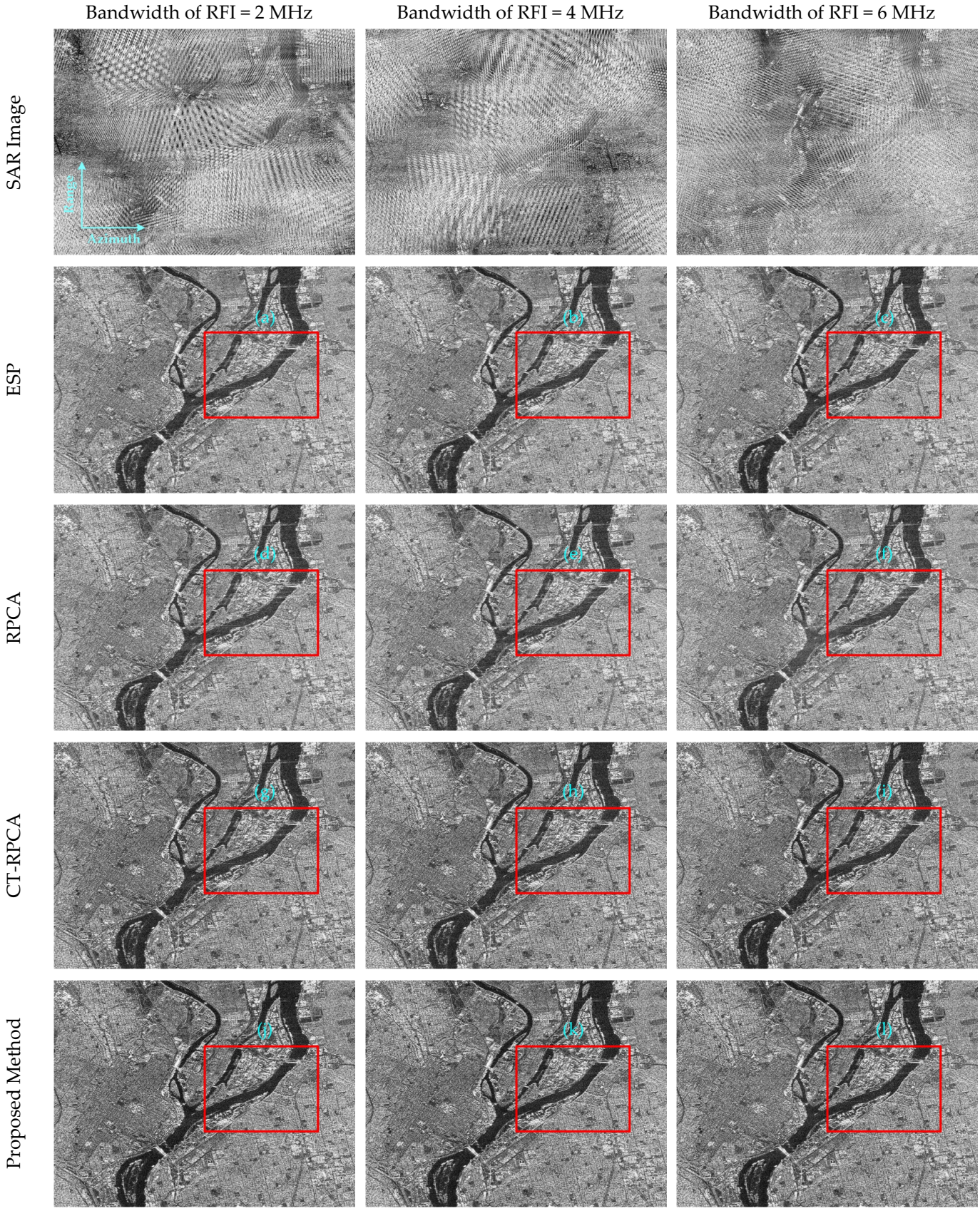

Figure 8. Mitigation performance for the ESP, RPCA, CT-RPCA, and proposed approach under different bandwidths of RFI. (**a**–**l**) ROIs for RFI mitigation results of different methods.

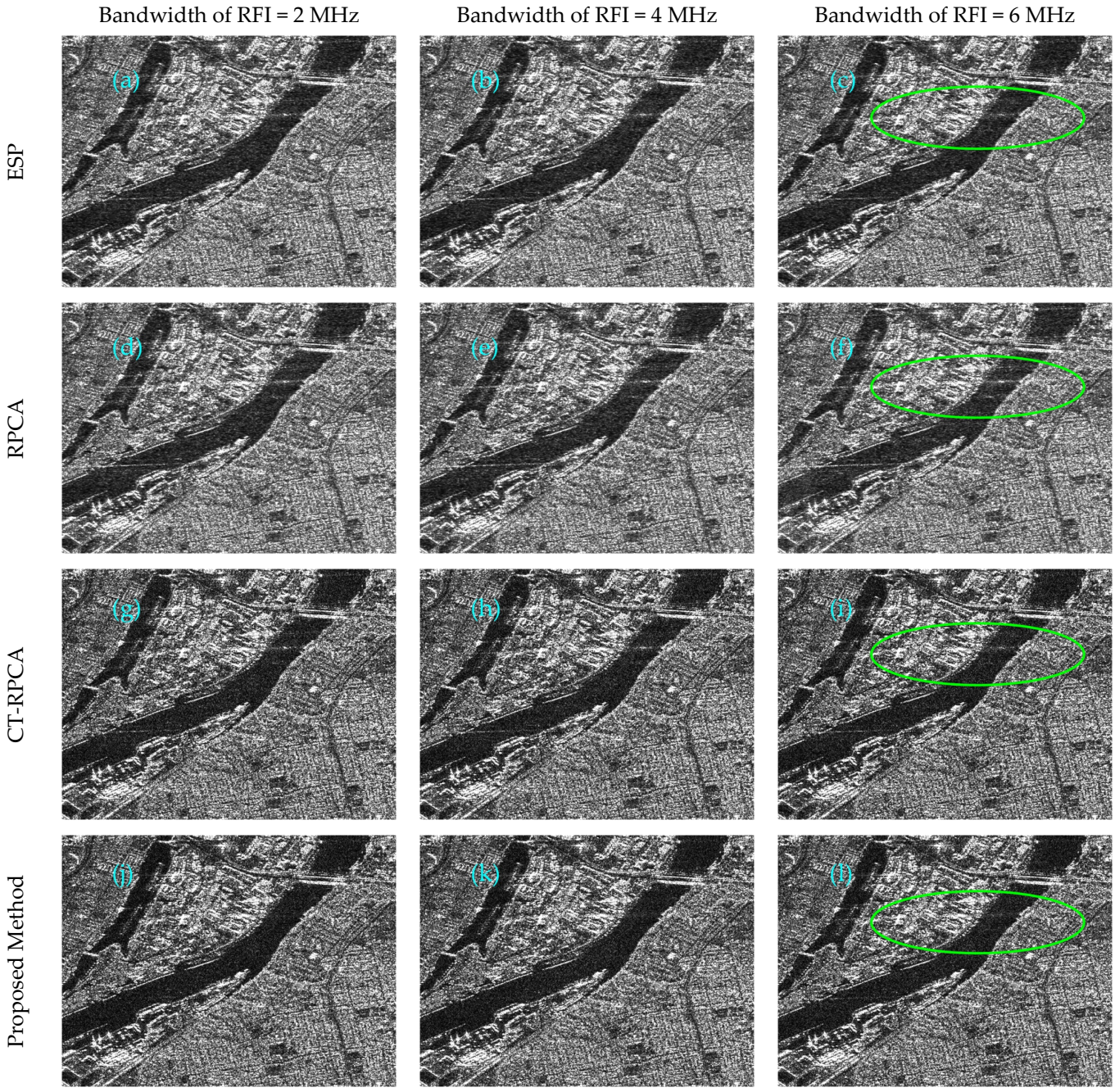

Figure 9. ROIs in Figure 8. (**a**–**c**) Mitigation results for the ESP method. (**d**–**f**) Mitigation results for the RPCA method. (**g**–**i**) Mitigation results for the CT-RPCA method. (**j**–**l**) Mitigation results for the proposed approach.

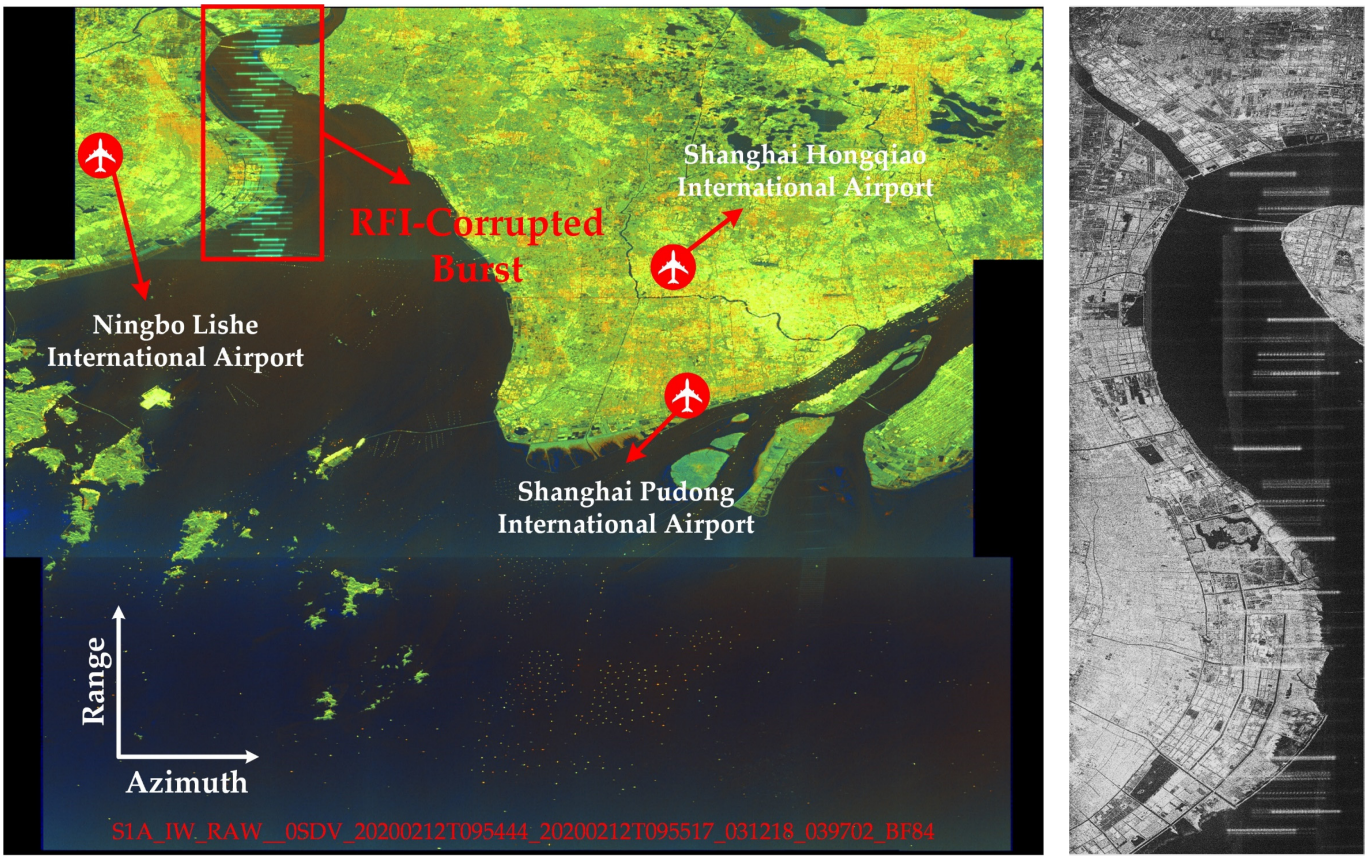

(**a**) (**b**)

Figure 10. RFI-contaminated image of the measured Sentinel-1 level-0 raw data: (**a**) The pseudo color image of the measured Sentinel-1 level-0 raw data; (**b**) The RFI-corrupted burst.

Further, the mitigation performance of the proposed method was analyzed using gray level entropy and average gradients. The entropy of the image can represent the distribution characteristics of the gray level in the image, indicating the texture complexity, which is defined as

$$E = -\sum_{k=1}^{L} P_k log_2(P_k) \tag{26}$$

where E represents the image entropy, L is the total gray level of the image, and P_k represents the probability of the occurrence of a pixel with a gray value of k. The average gradient is defined as

$$AG = \frac{\sum_{\tau=1}^{N_r}\sum_{\eta=1}^{N_a}\frac{1}{4}\sqrt{\left(\frac{\partial S(\tau,\eta)}{\partial \tau}\right)^2+\left(\frac{\partial S(\tau,\eta)}{\partial \eta}\right)^2}}{(N_r-1)(N_a-1)} \tag{27}$$

where $S(\tau,\eta)$ represents the position of the pixel in the SAR image, and $\partial S(\tau,\eta)/\partial\tau$ and $\partial S(\tau,\eta)/\partial\eta$ represent the grayscale gradient of the image in the vertical and horizontal directions, respectively.

The above experimental results show that all four methods can mitigate RFI with different performances. The ESP and RPCA methods are prone to abnormal side lobe effects when effectively removing RFI. The CT-RPCA method adds constraints when performing LRSD and can extract and mitigate RFI more effectively. However, it only decomposes the RFI in SAR signals once and has a limited ability to protect useful signals. Compared with the above three methods, the method proposed in this study has a better signal protection ability while effectively removing RFI, consistent with the previous results in this section. Table 4 shows the evaluation metrics for the four methods. It can be seen that the gray

level entropy and the average gradient of the proposed method are higher than ESP, RPCA, and CT-RPCA, which indicates that the proposed method can more effectively protect the useful signal while mitigating RFI.

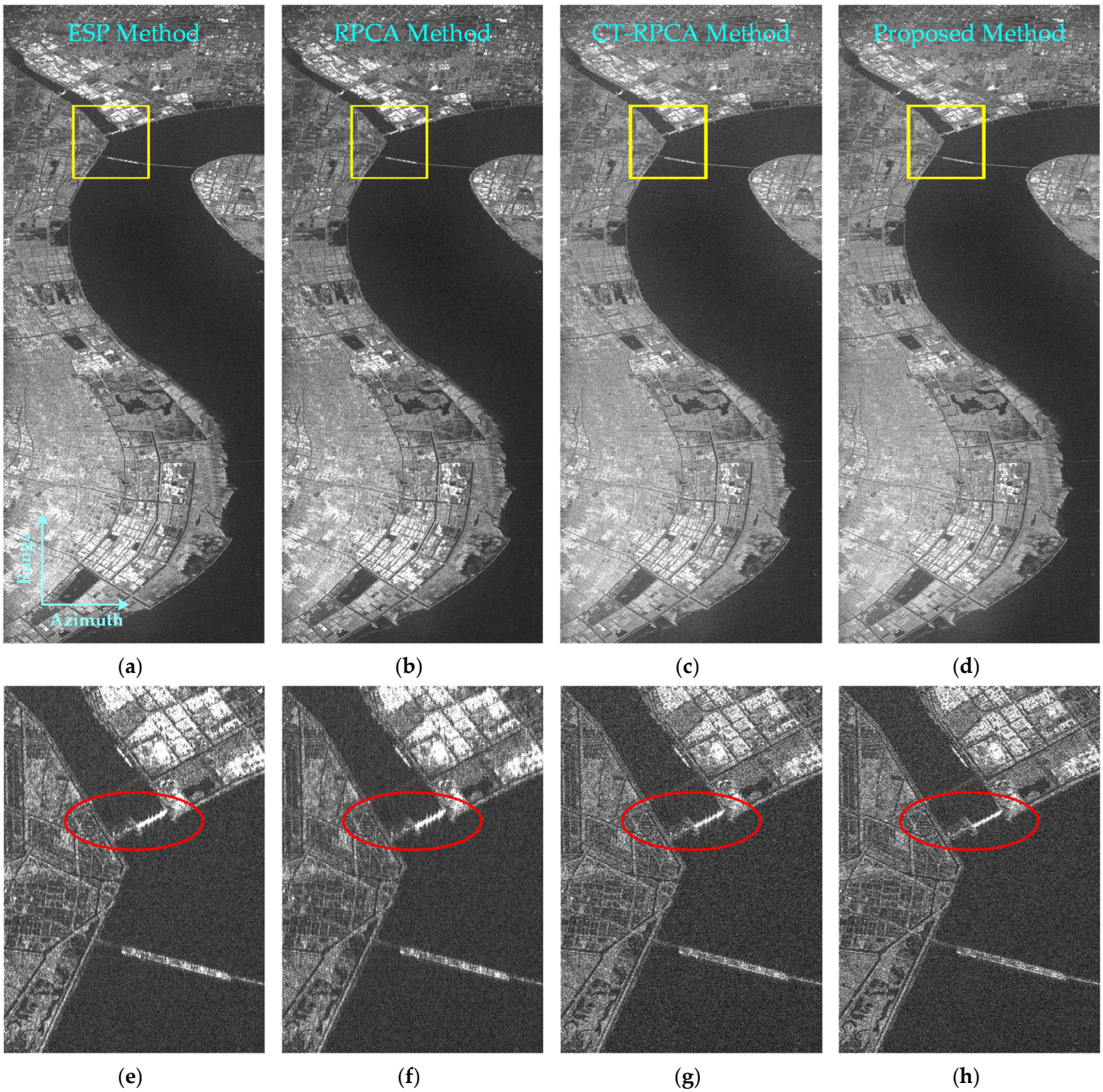

Figure 11. Experimental results for Sentinel-1 level-0 raw data: (**a**) Mitigation result by the ESP method; (**b**) Mitigation result by the RPCA method; (**d**) Mitigation result by the CT-RPCA method; (**c**) Mitigation result by the proposed approach; and (**e**–**h**) ROIs with the yellow box in (**a**–**d**).

Table 4. Gray level entropies and average gradients after ESP, RPCA, CT-RPCA, and proposed approach.

Metric \ Method	ESP	RPCA	CT-RPCA	Proposed Method
Gray Level Entropy	2.7351	2.2473	3.0627	**3.1969**
Average Gradient	2517.2639	2384.9916	2521.8028	**2550.0796**

The best results in each metric are highlighted in bold.

5. Conclusions

The existence of RFI seriously hinders SAR signal processing and image interpretation. However, most existing methods focused on the effective mitigation of RFI, but the protection of the useful signal was insufficient. To solve this problem, this article analyzed the characteristics of RFI in the frequency domain in detail. A mitigation method of RFI with a signal protection capability was proposed, including three steps, i.e., RFI detection, RFI extraction, and RFI secondary separation.

In the proposed method, the kurtosis coefficient was used to detect the RFI pulse-by-pulse in the range frequency domain. The preliminary RFI extraction was realized by performing LRSD on the echo matrix containing RFI. Then, a binary masking matrix was generated based on the extraction result of RFI, and the RFI and remaining useful signal in the low-rank matrix were separated again. The useful signal was reconstructed to complete the interference mitigation work. Compared with the traditional RFI mitigation method, the proposal considered both the RFI mitigation effect and the protection of useful signals simultaneously. The experimental results based on simulated and measured SAR data showed that this method can protect the useful signal more effectively than the ESP, RPCA, and CT-RPCA methods while mitigating RFI.

It is worth noting that protecting useful signals during the mitigation process is as necessary as the RFI mitigation effect. Otherwise, the loss of useful signals will reduce the resolution of SAR images. The proposed method can effectively reduce the loss of useful signals by secondary separation of the RFI extraction results and has great potential in RFI mitigation and useful signal protection. The authors hope that the proposed method can become a valuable tool to solve the RFI problem.

Author Contributions: Formal analysis, H.Z.; methodology, H.Z., J.C. and N.L.; validation, H.Z., L.M., J.L. and J.C.; resources, H.Z., Z.G. and N.L.; writing-original draft, H.Z. and L.M.; writing-review and editing, L.M., J.L., J.C., Z.G. and N.L.; funding acquisition, N.L.; All authors have read and agreed to the published version of the manuscript.

Funding: This work was supported in part by the National Natural Science Foundation of China under Grant 61871175; in part by the Foundation of Key Laboratory of Radar Imaging and Microwave Photonics, Ministry of Education, under Grant RIMP2020003; and in part by the Graduate Education Innovation and Quality Improvement Program of Henan University under Grant SYL20060144.

Data Availability Statement: Not applicable.

Acknowledgments: Thanks to all anonymous reviewers and editors for their comments and suggestions, making this article's content more rigorous and meaningful. In the meantime, the authors would like to express their gratitude to ESA for their open-source data of Sentinel-1 spaceborne SAR, which underpinned the validation experiments in this study.

Conflicts of Interest: The authors declare no conflict of interest.

References

1. Reigber, A.; Scheiber, R.; Jager, M.; Prats-Iraola, P.; Hajnsek, I.; Jagdhuber, T.; Papathanassiou, K.P.; Nannini, M.; Aguilera, E.; Baumgartner, S. Very-High-Resolution Airborne Synthetic Aperture Radar Imaging: Signal Processing and Applications. *Proc. IEEE* **2013**, *101*, 759–783. [CrossRef]
2. Moreira, A.; Prats-Iraola, P.; Younis, M.; Krieger, G.; Hajnsek, I.; Papathanassiou, K.P. A tutorial on Synthetic Aperture Radar. *IEEE Geosci. Remote Sens. Mag.* **2013**, *1*, 6–43. [CrossRef]
3. Deng, Y.; Yu, W.; Zhang, H.; Wang, W.; Liu, D.; Wang, R. Forthcoming Spaceborne SAR Development. *J. Radars* **2020**, *9*, 1–33.

4. Zhou, F.; Tao, M. Research on Methods for Narrow-Band Interference Suppression in Synthetic Aperture Radar Data. *IEEE J. Sel. Top. Appl. Earth Obs. Remote Sens.* **2015**, *8*, 3476–3485. [CrossRef]
5. Li, N.; Lv, Z.; Guo, Z. Observation and Mitigation of Mutual RFI Between SAR Satellites: A Case Study Between Chinese GaoFen-3 and European Sentinel-1A. *IEEE Trans. Geosci. Remote Sens.* **2022**, *60*, 5112819. [CrossRef]
6. Li, N.; Lv, Z.; Guo, Z. Pulse RFI Mitigation in Synthetic Aperture Radar Data via a Three-Step Approach: Location, Notch, and Recovery. *IEEE Trans. Geosci. Remote Sens.* **2022**, *60*, 5225617. [CrossRef]
7. Lv, Z.; Zhang, H.; Li, N.; Guo, Z. A Two-Step Approach for Pulse RFI Detection in SAR Data. In Proceedings of the 2021 IEEE Sensors, Sydney, Australia, 31 October–3 November 2021; pp. 1–4.
8. Su, J.; Tao, H.; Tao, M.; Wang, L.; Xie, J. Narrow-band Interference Suppression via RPCA-Based Signal Separation in Time–Frequency Domain. *IEEE J. Sel. Top. Appl. Earth Obs. Remote Sens.* **2017**, *10*, 5016–5025. [CrossRef]
9. Deng, Y.; Zhao, F.; Wang, Y. Brief Analysis on The Development and Application of Spaceborne SAR. *J. Radars* **2012**, *1*, 1–10. [CrossRef]
10. Lu, X.; Su, W.; Yang, J.; Gu, H.; Zhang, H.; Yu, W.; Yeo, T.S. Radio Frequency Interference Suppression for SAR via Block Sparse Bayesian Learning. *IEEE J. Sel. Top. Appl. Earth Obs. Remote Sens.* **2018**, *11*, 4835–4847. [CrossRef]
11. Yang, H.; He, Y.; Du, Y.; Zhang, T.; Yin, J.; Yang, J. Two-Dimensional Spectral Analysis Filter for Removal of LFM Radar Interference in Spaceborne SAR Imagery. *IEEE Trans. Geosci. Remote Sens.* **2022**, *60*, 5219016. [CrossRef]
12. Huang, Y.; Liao, G.; Zhang, L.; Xiang, Y.; Li, J.; Nehorai, A. Efficient Narrowband RFI Mitigation Algorithms for SAR Systems with Reweighted Tensor Structures. *IEEE Trans. Geosci. Remote Sens.* **2019**, *57*, 9396–9409. [CrossRef]
13. Huang, Y.; Wen, C.; Chen, Z.; Chen, J.; Liu, Y.; Li, J.; Hong, W. HRWS SAR Narrowband Interference Mitigation Using Low-Rank Recovery and Image-Domain Sparse Regularization. *IEEE Trans. Geosci. Remote Sens.* **2022**, *60*, 5217914. [CrossRef]
14. Huang, Y.; Liao, G.; Li, J.; Xu, J. Narrowband RFI Suppression for SAR System via Fast Implementation of Joint Sparsity and Low-Rank Property. *IEEE Trans. Geosci. Remote Sens.* **2018**, *56*, 2748–2761. [CrossRef]
15. Tao, M.; Su, J.; Huang, Y.; Wang, L. Mitigation of Radio Frequency Interference in Synthetic Aperture Radar Data: Current Status and Future Trends. *Remote Sens.* **2019**, *11*, 2438. [CrossRef]
16. Huang, Y.; Zhao, B.; Tao, M.; Chen, Z.; Hong, W. Review of Synthetic Aperture Radar Interference Suppression. *J. Radars* **2020**, *9*, 86–106.
17. Braunstein, M.; Ralston, J.; Sparrow, D. Signal Processing Approaches to Radio Frequency Interference (RFI) Suppression. In Proceedings of the Algorithms for Synthetic Aperture Radar Imagery, Proceedings of the SPIE 2230, Orlando, FL, USA, 9 June 1994; pp. 190–208.
18. Huang, X.; Liang, D. RFI Suppression in UWB-SAR based on RELAX. *Natl. Univ. Def. Technol. J.* **2000**, *22*, 55–59.
19. Huang, X.; Liang, D. Parametric Methods of RFI Suppression in UWB-SAR. *Syst. Eng. Electron.* **2000**, *22*, 94–97.
20. Liu, Z.; Liao, G.; Yang, Z. Time Variant RFI Suppression for SAR Using Iterative Adaptive Approach. *IEEE Geosci. Remote Sens. Lett.* **2013**, *10*, 1424–1428. [CrossRef]
21. Yang, Z.; Du, W.; Liu, Z.; Liao, G. WBI Suppression for SAR Using Iterative Adaptive Method. *IEEE J. Sel. Top. Appl. Earth Obs. Remote Sens.* **2016**, *9*, 1008–1014. [CrossRef]
22. Han, W.; Bai, X.; Fan, W.; Wang, L.; Zhou, F. Wideband Interference Suppression for SAR via Instantaneous Frequency Estimation and Regularized Time-Frequency Filtering. *IEEE Trans. Geosci. Remote Sens.* **2022**, *60*, 5208612. [CrossRef]
23. Cazzaniga, G.; Guarnieri, A.M. Removing RF Interferences from P-band Airplane SAR Data. In Proceedings of the IGARSS' 96, Lincoln, NE, USA, 31 May 1996; pp. 1845–1847.
24. Xu, W.; Xing, W.; Fang, C.; Huang, P.; Tan, W. RFI Suppression Based on Linear Prediction in Synthetic Aperture Radar Data. *IEEE Geosci. Remote Sens. Lett.* **2021**, *18*, 2127–2131. [CrossRef]
25. Li, N.; Lv, Z.; Guo, Z.; Zhao, J. Time-Domain Notch Filtering Method for Pulse RFI Mitigation in Synthetic Aperture Radar. *IEEE Geosci. Remote Sens. Lett.* **2021**, *19*, 4013805. [CrossRef]
26. Vu, V.T.; Sjögren, T.K.; Pettersson, M.I.; Håkansson, L.; Gustavsson, A.; Ulander, L.M.H. RFI Suppression in Ultrawideband SAR Using an Adaptive Line Enhancer. *IEEE Geosci. Remote Sens. Lett.* **2010**, *7*, 694–698. [CrossRef]
27. Lamont-Smith, T.; Hill, R.; Hayward, S.; Yates, G.; Blake, A. Filtering Approaches for Interference Suppression in Low-Frequency SAR. *IEE Proc.-Radar Sonar Navig.* **2006**, *153*, 338–344. [CrossRef]
28. Zhou, F.; Wu, R.; Xing, M.; Bao, Z. Eigensubspace-Based Filtering with Application in Narrow-Band Interference Suppression for SAR. *IEEE Geosci. Remote Sens. Lett.* **2007**, *4*, 75–79. [CrossRef]
29. Zhou, F.; Tao, M.; Bai, X.; Liu, J. Narrow-Band Interference Suppression for SAR Based on Independent Component Analysis. *IEEE Trans. Geosci. Remote Sens.* **2013**, *51*, 4952–4960. [CrossRef]
30. Zhou, F.; Xing, M.; Bai, X.; Sun, G.; Bao, Z. Narrow-band Interference Suppression for SAR based on Complex Empirical Mode Decomposition. *IEEE Geosci. Remote Sens. Lett.* **2009**, *6*, 423–427. [CrossRef]
31. Tao, M.; Zhou, F.; Liu, J.; Liu, Y.; Zhang, Z.; Bao, Z. Narrow-Band Interference Mitigation for SAR Using Independent Subspace Analysis. *IEEE Trans. Geosci. Remote Sens.* **2014**, *52*, 5289–5301.
32. Feng, J.; Zheng, H.; Deng, Y.; Gao, D. Application of Subband Spectral Cancellation for SAR Narrow-Band Interference Suppression. *IEEE Geosci. Remote Sens. Lett.* **2012**, *9*, 190–193. [CrossRef]
33. Yang, H.; Li, K.; Li, J.; Du, Y.; Yang, J. BSF: Block Subspace Filter for Removing Narrowband and Wideband Radio Interference Artifacts in Single-Look Complex SAR Images. *IEEE Trans. Geosci. Remote Sens.* **2022**, *60*, 5211916. [CrossRef]

34. Li, N.; Lv, Z.; Guo, Z. SAR Image Interference Suppression Method by Integrating Change Detection and Subband Spectral Cancellation Technology. *Syst. Eng. Electron.* **2021**, *43*, 2484–2492.
35. Guo, Y.; Liao, G.; Li, J.; Chen, X. A Novel Moving Target Detection Method Based on RPCA for SAR Systems. *IEEE Trans. Geosci. Remote Sens.* **2020**, *58*, 6677–6690. [CrossRef]
36. Yang, D.; Yang, X.; Liao, G.; Zhu, S. Strong Clutter Suppression via RPCA in Multichannel SAR/GMTI System. *IEEE Geosci. Remote Sens. Lett.* **2015**, *12*, 2237–2241. [CrossRef]
37. Guo, Y.; Liao, G.; Li, J.; Gu, T. A Clutter Suppression Method Based on NSS-RPCA in Heterogeneous Environments for SAR-GMTI. *IEEE Trans. Geosci. Remote Sens.* **2020**, *58*, 5880–5891. [CrossRef]
38. Oveis, A.H.; Sebt, M.A. Dictionary-Based Principal Component Analysis for Ground Moving Target Indication by Synthetic Aperture Radar. *IEEE Geosci. Remote Sens. Lett.* **2017**, *14*, 1594–1598. [CrossRef]
39. Leibovich, M.; Papanicolaou, G.; Tsogka, C. Low Rank Plus Sparse Decomposition of Synthetic Aperture Radar Data for Target Imaging. *IEEE Trans. Comput. Imaging* **2020**, *6*, 491–502. [CrossRef]
40. Nguyen, L.H.; Tran, T.; Do, T. Sparse Models and Sparse Recovery for Ultra-Wideband SAR Applications. *IEEE Trans. Aerosp. Electron. Syst.* **2014**, *50*, 940–958. [CrossRef]
41. Liu, H.; Li, D.; Zhou, Y.; Truong, T.K. Joint Wideband Interference Suppression and SAR Signal Recovery Based on Sparse Representations. *IEEE Geosci. Remote Sens. Lett.* **2017**, *14*, 1542–1546. [CrossRef]
42. Huang, Y.; Liao, G.; Xiang, Y.; Zhang, Z.; Li, J.; Nehorai, A. Reweighted Nuclear Norm and Reweighted Frobenius Norm Minimizations for Narrowband RFI Suppression on SAR System. *IEEE Trans. Geosci. Remote Sens.* **2019**, *57*, 5949–5962. [CrossRef]
43. Huang, Y.; Liao, G.; Zhang, Z.; Xiang, Y.; Li, J.; Nehorai, A. Fast Narrowband RFI Suppression Algorithms for SAR Systems via Matrix-Factorization Techniques. *IEEE Trans. Geosci. Remote Sens.* **2019**, *57*, 250–262. [CrossRef]
44. Huang, Y.; Zhang, L.; Li, J.; Hong, W.; Nehorai, A. A Novel Tensor Technique for Simultaneous Narrowband and Wideband Interference Suppression on Single-Channel SAR System. *IEEE Trans. Geosci. Remote Sens.* **2019**, *57*, 9575–9588. [CrossRef]
45. Yang, H.; Chen, C.; Chen, S.; Xi, F.; Liu, Z. A Dictionary-Based SAR RFI Suppression Method via Robust PCA and Chirp Scaling Algorithm. *IEEE Geosci. Remote Sens. Lett.* **2021**, *18*, 1229–1233. [CrossRef]
46. Joy, S.; Nguyen, L.H.; Tran, T.D. Joint Down-Range and Cross-Range RFI Suppression in Ultra-Wideband SAR. *IEEE Trans. Geosci. Remote Sens.* **2021**, *59*, 3136–3149. [CrossRef]
47. Zhang, H.; Huang, Y.; Li, J.; Chen, Z.; Cai, L.; Hong, W. Time-Varying RFI Mitigation for SAR Systems via Graph Laplacian Clustering Techniques. *IEEE Geosci. Remote Sens. Lett.* **2022**, *19*, 4010805. [CrossRef]
48. Ding, Y.; Fan, W.; Zhang, Z.; Zhou, F.; Lu, B. Radio Frequency Interference Mitigation for Synthetic Aperture Radar Based on the Time-Frequency Constraint Joint Low-Rank and Sparsity Properties. *Remote Sens.* **2022**, *14*, 775. [CrossRef]
49. Akeret, J.; Chang, C.; Lucchi, A.; Refregier, A. Radio Frequency Interference Mitigation Using Deep Convolutional Neural Networks. *Astron. Comput.* **2017**, *18*, 35–39. [CrossRef]
50. Fan, W.; Zhou, F.; Tao, M.; Bai, X.; Rong, P.; Yang, S.; Tian, T. Interference Mitigation for Synthetic Aperture Radar Based on Deep Residual Network. *Remote Sens.* **2019**, *11*, 1654. [CrossRef]
51. Tao, M.; Li, J.; Su, J.; Wang, L. Characterization and Removal of RFI Artifacts in Radar Data via Model-Constrained Deep Learning Approach. *Remote Sens.* **2022**, *14*, 1578. [CrossRef]
52. Zhou, C.; Li, F.; Li, N.; Zheng, H.; Wang, R. Improved Eigensubspace-based Approach for Radio Frequency Interference Filtering of Synthetic Aperture Radar Images. *J. Appl. Remote Sens.* **2017**, *11*, 025004. [CrossRef]
53. Shang, R.; Lin, J.; Jiao, L.; Li, Y. SAR Image Segmentation Using Region Smoothing and Label Correction. *Remote Sens.* **2020**, *12*, 803. [CrossRef]